# Local structures and temperature-driven polarization rotation in Zr-rich $PbZr_{1-x}Ti_xO_3$

Zhen Wang, Nan Zhang, Hiroko Yokota, A. M. Glazer, Yasuhiro Yoneda, Wei Ren, and Zuo-Guang Ye

Citation: Appl. Phys. Lett. **113**, 012901 (2018); doi: 10.1063/1.5024422
View online: https://doi.org/10.1063/1.5024422
View Table of Contents: http://aip.scitation.org/toc/apl/113/1
Published by the American Institute of Physics

# Local structures and temperature-driven polarization rotation in Zr-rich $PbZr_{1-x}Ti_xO_3$

Zhen Wang,[1] Nan Zhang,[1,a)] Hiroko Yokota,[2,b)] A. M. Glazer,[3,c)] Yasuhiro Yoneda,[4] Wei Ren,[1] and Zuo-Guang Ye[1,5]

[1]*Electronic Materials Research Laboratory, Key Laboratory of the Ministry of Education & International Center for Dielectric Research, School of Electronic and Information Engineering, Xi'an Jiaotong University, Xi'an 710049, People's Republic of China*
[2]*Department of Physics, Chiba University, 1-33 Yayoi-cho, Inage-ku, Chiba City 263-8522, Japan*
[3]*Department of Physics, University of Oxford, Parks Road, Oxford OX1 3PU, England*
[4]*Reaction Dynamics Research Division, Japan Atomic Energy Agency (JAEA), Sayo, Hyogo 679-5148, Japan*
[5]*Department of Chemistry and 4D LABS, Simon Fraser University, 8888 University Drive, Burnaby, British Columbia V5A 1S6, Canada*

(Received 1 February 2018; accepted 7 June 2018; published online 2 July 2018)

$PbZr_{1-x}Ti_xO_3$, which has abundant structural variations in the corresponding physical properties, has been used in a large variety of applications. To understand the effect of the structure on its high-performance piezoelectric properties, its local and average structures are studied. Total scattering data have been obtained from high-energy synchrotron powder diffraction experiments at 20 K and 300 K. Using the reverse Monte Carlo method, information on cation displacements has been extracted from X-ray Pair Distribution Function data. This suggests that the local disorder of the B cations is mainly driven by thermal motion, while the local disorder of Pb is most likely caused by more complex factors, such as displacive disorder. Both rhombohedral and monoclinic local polarizations are observed in Zr-rich PZT, whose directions depend on temperature. *Published by AIP Publishing.* https://doi.org/10.1063/1.5024422

Lead zirconate-titanate ($PbZr_{1-x}Ti_xO_3$: PZT) is one of the most widely-used piezoelectric materials in industrial, military and general applications because of its high electromechanical coupling and piezoelectric constant. The global market for piezoelectric operated actuators and motors is estimated to reach $31.33 billion by 2022, showing an annual growth rate of 4.88%.[1] PZT belongs to the perovskite $ABX_3$ family. It is a solid solution of antiferroelectric lead zirconate $PbZrO_3$ and ferroelectric lead titanate $PbTiO_3$. At a Ti concentration of 48%, there is an almost vertical boundary known as the morphotropic phase boundary (MPB).[2,3] Around the MPB, the piezoelectric constant and electromechanical coupling coefficients exhibit maximum values. It had been a mystery for a long time as to why this is so, especially given the lack of a group-subgroup relationship between the Zr-rich rhombohedral (*R*3*m*/*R*3*c*) and Ti-rich tetragonal (*P*4*mm*) phases. The discovery of a monoclinic *Cm* phase, which acts as the "bridge" between these two phases, provided an explanation for the enhanced piezoelectric response by the so-called "polarization rotation mechanism" described from first-principles calculations.[4–6] This model suggests that a lower-symmetry phase is important in realizing the enhancement of physical properties, since in such a case the spontaneous polarization is free to rotate within a mirror plane. Nowadays, the existence of a long-range monoclinic phase in the MPB region has been widely accepted and the concept of the MPB has been adopted in many solid-solution systems to achieve giant piezoelectric responses.

In our previous work, we have found that the average structure of PZT in a wide composition range, even far away from the MPB, is still complex, and the presence of monoclinic distortion is frequently found alongside the major rhombohedral *R*3*m*/*R*3*c* phase.[7,8] Therefore, in the study of the PZT structure, conventional diffraction methods, which reveal only the average structure, are not enough. It is necessary to extend the structural study to the local scale. In our neutron scattering experiments, it was revealed that local monoclinic components exist in many compositions at room temperature. A short-range displacement change corresponding to those expected in monoclinic $M_B$-$M_A$ phases was identified on the "rhombohedral" side of the MPB region,[9] where the Pb displacements point away from [111] but are free to rotate within the (110) plane. On the "tetragonal" side close to the MPB, the correlation length of the $M_A$ component decreases and more cations are displaced in the (100) plane corresponding to an $M_C$ phase.[10] (The definition and structural details of the $M_A$, $M_B$ and $M_C$ monoclinic types can be found in Vanderbilt and Cohen.[11]) In the Zr-rich compositions of PZT, the polarization remains along ⟨111⟩ in the average rhombohedral structure from low-temperatures up to $T_C$ (here and throughout the paper, we use the pseudocubic cell setting for the crystallographic directions). However, with the discovery of the short-range displacements corresponding to those in a monoclinic phase, it is essential to investigate any possible short-range structural change and polarization rotation with changing temperature.

Our previous investigations on PZT further demonstrated the importance of local structural studies in functional oxides.[12] Other examples include relaxor materials, which exhibit characteristic behaviors such as dielectric dispersion,

a)Email: nzhang1@xjtu.edu.cn
b)Email: hiroko.9bq@chiba-u.jp
c)Email: mike.glazer@jesus.ox.ac.uk

non-ergodicity and diffuse scattering. They have been thought to possess local structures that are different from the average structure in the form of so-called polar nanoregions (PNRs)[13] embedded in a cubic matrix. Local symmetry breaking distortions have also been reported in classical ferroelectrics such as in $BaTiO_3$ by neutron analysis,[14] Brillouin light scattering,[15] temperature dependence of the refractive index[16] and second harmonic generation.[17] A common method used to probe the local structure is that of total scattering,[18,19] which incorporates both Bragg and diffuse scattering intensities. The Fourier transform of the normalized total scattering intensity gives the pair distribution function (PDF),[20,21] which describes the probability of finding any two atoms at a given inter-atomic distance. Previously, short-range structures of crystalline materials were usually investigated using neutron total scattering. However, in recent years, third-generation synchrotron radiation sources enable us to study the local structure using X-ray diffraction techniques by measuring the X-ray total scattering data.[22–24] Here, we present a local structural study of PZT ($x = 0.25$) as a function of temperature based on the reverse Monte Carlo (RMC)[25] modeling of the X-ray pair distribution function (XPDF) data. By analyzing the Pb displacement in each unit cell, we show that this Zr-rich PZT consists of a mixture of rhombohedral and monoclinic *local* polarizations that change direction with temperature.

A PZT ($x = 0.25$) powder sample was prepared by the mixed oxide method. The details of sample preparation can be found in Ref. 7. The sample quality was checked by X-ray diffraction using a P′Analytical X'PERT powder diffractometer and neither secondary nor impurity phases were detected. For the synchrotron experiment, the powder sample was packed into Kapton polyimide tubes with a diameter of 1 mm. High-energy X-ray powder diffraction data were collected up to a high momentum transfer $Q = 25\,Å^{-1}$ and a Q resolution of $0.01564\,Å^{-1}$ using 60 keV (wavelength = 0.206502 Å) X-rays at the BL14B1 beamline at SPring-8.[26] Since the X-ray scattering cross-sections are Q-dependent, the intensity drops off significantly with Q. To compensate this Q-dependence, we divided the Q range that was measured into four parts with different data collection times. In the high-Q range, we increased the data collection time in order to collect enough intensity. The experiments were performed at 300 K and 20 K. Since there is no obvious average structural change for this composition below $T_C$, we chose the highest and lowest temperatures that we can achieve in this experiment. The diffraction data were normalized and merged into a single full pattern. This was corrected for absorption, multiple scattering and polarization effects. The background and Compton scattering were removed. The data reduction was done using software PDFgetX2.[27]

We first compare the X-ray pair distribution function (XPDF) with the neutron PDF data from a similar composition,[9] as shown in Fig. 1. The very short-range data at a distance $r$ from 0 to 5 Å are shown in Fig. 1(b). Despite the fact that the overall patterns for neutron and X-ray data appear to be different, they do express the same information about the local structures when the bonds are formed between the cations. In Fig. 1(b), there are several peaks in the neutron PDF, such as the negative Ti-O peaks around $r = 1.80$ Å (the neutron scattering length for Ti is negative), with positive Zr-O, Pb-O and O-O peaks around $r = 2.08$, 2.414, and 2.88 Å, respectively, that are very weak in the XPDF profile. It is well known that X-rays are not sensitive to light atoms such as oxygen. Therefore, the neutron PDF gives more accurate measurements of the A-O, B-O and O-O bonds, while the relative displacements between A and B cations are more clearly observed as variable A-B pairs in the XPDF data.

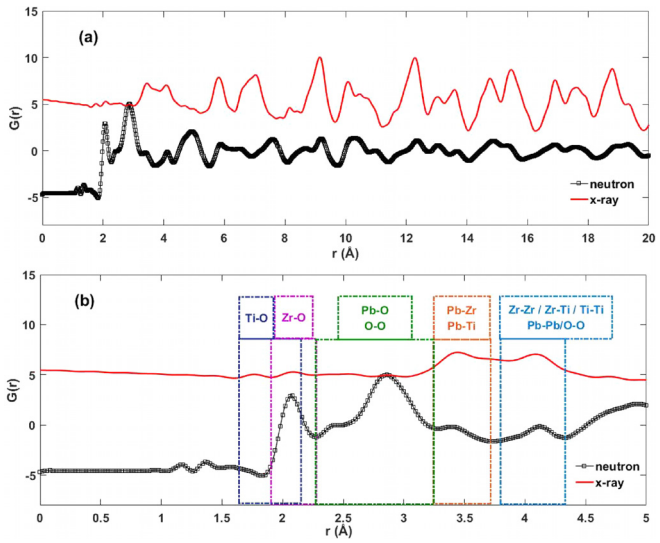


FIG. 1. (a) PDF profiles measured at room temperature. For comparison, neutron PDF data are shown in black. An enlargement of (a) is shown in (b) with the range of the major bonds outlined in the colored boxes. The ranges for Ti-O and Zr-O are shown overlapping.

The experimental XPDF data for PZT ($x = 0.25$) at 20 K and 300 K are compared in Fig. 2. It is worth noting that the peaks at 20 K are sharper than those observed at room temperature. This is not surprising since the atomic thermal motion becomes more active with the increase of temperature. Although the peak widths are broader at 300 K, their positions do not shift much. However, the peaks around $r = 3.45$ Å (corresponding to the A-B bonds) and 4.11 Å (corresponding to the A-A/B-B bonds) have different shapes at 20 K and 300 K, indicating a possible local structural change with temperature.

The PDF data were firstly analyzed by the small-box modeling method using software PDFFIT.[28] Single rhombohedral *R*3*m* and monoclinic *Cm* structural restrictions were

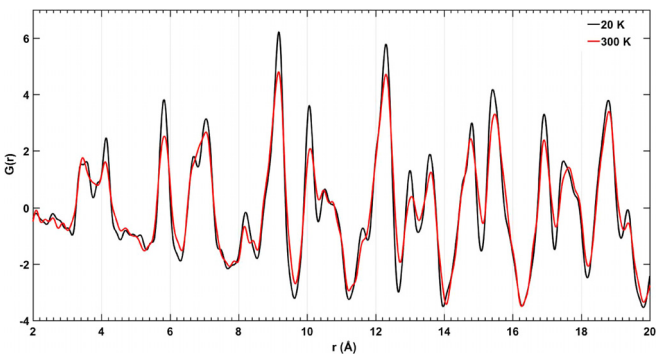


FIG. 2. Experimental XPDF patterns for PZT ($x = 0.25$) at 20 K (black line) and 300 K (red line).

applied during the refinement process for both the 300 K and 20 K patterns. The oxygens were fixed at their ideal positions because of the small X-ray scattering cross-section. Above 8 Å, both models reproduce the PDF profile well, while in the short range below 8 Å, there are several small, but nevertheless real, discrepancies between the experimental data and the calculation [see supplementary material Figs. S1(a) and S1(b)]. The best fit was obtained when the oxygen positions were also refined but then the resulting structure exhibited large unrealistic distortions.

To analyze the element-specific local structural details, we carried out the RMC simulation using software RMCProfile.[29,30] In the RMCProfile algorithm, the Q-dependence of the X-ray scattering cross-sections is taken into account as normalized Faber-Ziman coefficients and the Q-dependent partial structure factors are contained within the F($Q$) data file for the program to use during the refinement.[31] We used a configuration of $10 \times 10 \times 10$ pseudocubic unit cells with the starting rhombohedral ($R3c$) structural model obtained from the Rietveld refinement of the Bragg profiles. The experimental XPDF G($r$), the total scattering intensity F($Q$)[18] and the Bragg profile data were refined at the same time with the distance window constraints and bond valence constraints being applied. Since the limited $r$ range in the configuration causes the broadening of the Bragg peaks in the calculated F($Q$), in RMCProfile, the experimental F($Q$) was degraded by convolution with a box function defined by the dimension of the box size before being compared with the calculated pattern.[29] The experimental and calculated RMC patterns of G($r$), F($Q$), Bragg intensities and partial PDFs at 20 K and 300 K are displayed in Figs. S1(c)–S1(j), which show that the RMC modeling gives an excellent fit to the observed data. After the RMC modeling, the partial PDF pairs containing heavy elements that are sensitive to X-rays are obtained and shown in Fig. 3 for the region from 3 to 5 Å. At 20 K, the peak for the Pb-Pb atom pair is sharp and strong, as seen in Fig. 3(a); but the peak becomes much wider and lower when the temperature is increased up to 300 K [Fig. 3(b)]. The same phenomenon is demonstrated more clearly in Figs. 3(c) and 3(d), showing a comparison between the Pb-Pb and Zr-Zr bonds at 20 K and 300 K. (The reason that we only plot the peak for the Zr-Zr bond for comparison is that 75% of the B sites are occupied by Zr, and so the Zr-Zr bond gives better statistics than the Zr-Ti or Ti-Ti bonds.) The peak width of the Zr-Zr pairs increases slightly as the temperature is increased from 20 K to 300 K and the peak shapes are almost the same, which indicates that the disorder of Zr is at a low level and is probably isotropic, possibly owing to weak thermal motion. However, the Pb-Pb peak width increases significantly, and at the same time, two shoulders around the major peak emerge at 300 K. This suggests a far more anisotropically disordered local distribution for Pb, which should be related to more complex factors besides thermal disorder, e.g., displacive disorder. This is in good agreement with the previous high-resolution neutron powder diffraction data and the corresponding Rietveld refinement results of Zr-rich PZT, which show that from 8 K to 300 K, the isotropic displacement parameter ($B_{iso}$) of Zr/Ti increased from 0.31(1) Å$^2$ to 0.60(3) Å$^2$, while that of Pb increased much more, from 0.800(8) Å$^2$ to 2.11(3) Å$^2$,[8] which cannot simply arise from thermal motion alone.

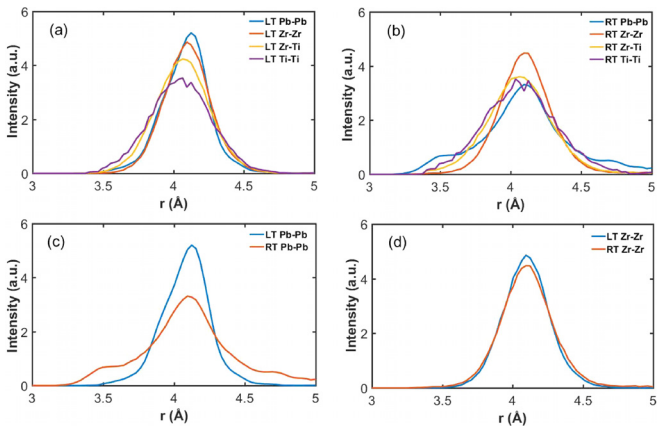


FIG. 3. Partial PDFs of the Pb-Pb, Zr-Zr, Zr-Ti, and Ti-Ti atom pairs in the region of 3–5 Å for (a) 20 K and (b) 300 K. (c) A comparison of the Pb-Pb bonds and (d) the Zr-Zr bonds at 20 K and 300 K.

The obtained models have also been statistically analyzed in order to identify the direction of atomic displacements of the Pb cations. In the neutron measurements, the Pb cation displacements are calculated against the center of the oxygen octahedra. However, this is unsuitable for XPDF since the X-rays are insensitive to the light atoms and the effect of Q-dependence on X-ray scattering cross-sections is more noticeable for oxygens. Therefore, the displacement directions are calculated as vectors between the centroid position of the surrounding B cations and the Pb positions in the RMC-refined structural models, because the displacements of Zr/Ti are relatively small, about 1/3 of the Pb displacements in the PZT solid solutions.[7,8] Also, because of the relatively large displacement lengths of Pb, the local polarizations are mainly due to the Pb displacements. This is especially true at this PZT composition, where the percentage of Zr on the B-site is high (75%) and it is known that Zr is usually considered to be ferroelectrically inactive.[10] The distributions of the Pb displacement directions are plotted in the form of stereographic projections, which is a convenient way to distinguish displacements along the rhombohedral (R, ⟨111⟩), tetragonal (T, ⟨001⟩), orthorhombic (O, ⟨110⟩) symmetry axes, or within a monoclinic (M, {110}/{100}) mirror plane. The statistical results in Fig. S2 and Figs. 4(a) and 4(b) show that at 20 K the Pb cations are displaced predominantly along ⟨111⟩, with a small amount on the {110} planes. Interestingly, both the $M_A$ (between ⟨111⟩ and ⟨001⟩) and $M_B$ (between ⟨111⟩ and ⟨110⟩) components are observed. Most of the angles between the Pb displacement directions and ⟨111⟩ are small [less than 5(±0.06)°]. At 300 K, the displacement directions of the Pb cations cover a larger area in the stereographic projection, which means that the degree of disorder, especially the displacive disorder, becomes stronger with the increase in temperature. In particular, there are fewer Pb atoms displaced exactly along ⟨111⟩ compared with the other directions on the {110} plane. Two maxima are observed on either side of ⟨111⟩, and the angles between the maxima of the Pb displacement vectors and ⟨111⟩ are larger [about 9(±0.08)°] than those at 20 K. This tendency is more clearly shown in Figs. 4(c) and 4(d), where

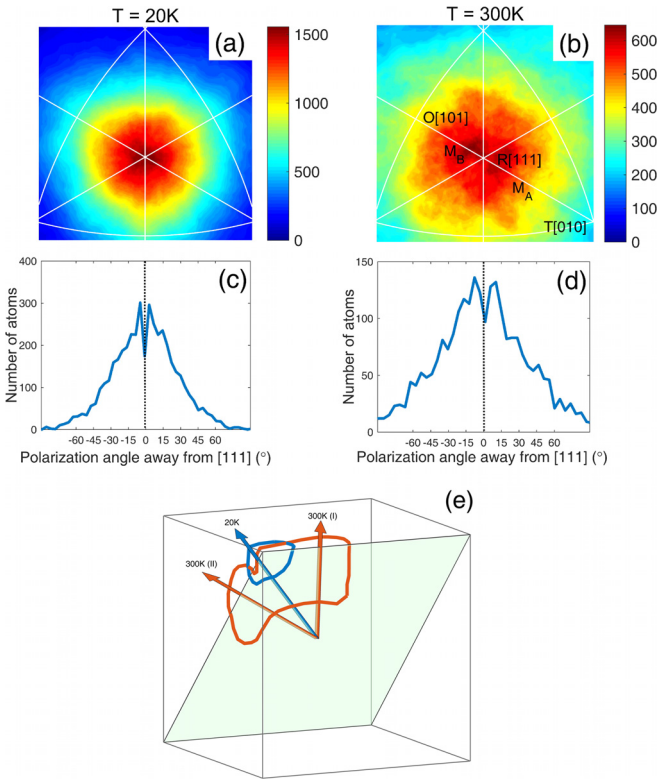


FIG. 4. (a) and (b) Enlarged stereographic projection plots for the Pb atomic displacements obtained from the RMC calculation. (a) shows displacement directions at 20 K and (b) at 300 K. The viewing direction is down [111]. The R, T, and O points are marked on (b). Along the (110) mirror plane, the polarization of $M_A$ and $M_B$ can, in principle, rotate freely between the R and T points, or the R and O points, respectively. The possible $M_A$ and $M_B$ directions are also shown in (b). (c) and (d) are one-dimensional distribution profiles of the Pb atom displacement angles on one of the {110} planes away from [111] at 20 K and 300 K. (e) Schematic of the changes in the direction of Pb polarization within the monoclinic mirror plane from 20 K to 300 K. The contours are taken from the stereographic projections in (a) and (b) and projected onto the surface of a prototypic cube. The arrows indicate the predominant displacement directions.

we plot the 1-D distribution of the Pb displacement directions on the {110} plane. This indicates that local polarizations with R, $M_A$ and $M_B$ directions coexist at 20 K, and the proportion of the local polarizations pointing exactly along the rhombohedral symmetry axis decreases upon reaching room temperature. The increase in the angle between the Pb displacement vector and ⟨111⟩ with increasing temperature corresponds to a temperature-induced change in the polarization direction [shown in Fig. 4(e)]. Note that with the local polarization directions at only two temperatures, one cannot tell for sure whether the polarization rotation is continuous or not. To distinguish this, further studies at more temperatures will be necessary.

The stereographic projection plot shows a statistical distribution of the local Pb displacements. However, it does not provide information on correlations over a large length scale. Therefore, we calculated the displacement correlation coefficients of the neighboring *i*th and *j*th Pb atoms in each of the ***X***, ***Y***, and ***Z*** directions using the equation

$$c_{ij}^{x} = \frac{\langle x_i x_j \rangle}{\left( \langle x_i^2 \rangle \langle x_j^2 \rangle \right)^{1/2}}, \tag{1}$$

where $x_i$ is the displacement along the ***X*** axis of the *i*th Pb atom.[32] The average correlation coefficients calculated from 100 RMC runs at 20 K are 0.583(4), 0.568(5), and 0.589(4) in the ***X***, ***Y***, and ***Z*** directions. At 300 K, the coefficients in the ***X***, ***Y***, and ***Z*** directions are reduced to 0.323(4), 0.329(4), and 0.330(4), respectively. The histograms of the coefficients are shown in Figs. S3(a)–S3(f). This indicates that at both temperatures, certain levels of Pb-Pb displacement correlations exist.[33] An increase of the disordering level is observed at room temperature. Figure S3(g) shows part of the Pb displacement distributions in a three-dimensional space in a larger box of $20 \times 20 \times 20$ pseudocubic unit cells modeled by RMC at 20 K. A close examination shows that the displacement correlation exists mostly on the scale of 4–5 unit cells. Therefore, there is a collection of locally correlated monoclinic polarizations rather than a long-range "monoclinic phase" in this material. The polarization rotation that we have observed largely exists at the unit cell level, similar to the results of first-principles calculations.[5]

In this work, high-energy synchrotron diffraction experiments were carried out on PZT ($x = 0.25$) at 20 K and 300 K. With the help of the RMC method, information on the local structures was extracted from the X-ray PDF data. Although the average structures at 20 K and 300 K are both rhombohedral, the local Pb displacements are found to be increasingly driven away from the ⟨111⟩ directions as the temperature increases, so that both $M_A$ and $M_B$ local polarizations form at 300 K, indicating a local polarization rotation driven by changing temperature. In many Pb-based solid-solution systems including PZT, the existence of an average monoclinic phase has been observed at various temperatures around the MPB.[3,34,35] The monoclinic distortion is recognized as one of the most significant contributors to the high piezoelectric response, especially via polarization rotation under an electric field.[36,37] Although our present study focuses on the Zr-rich compositions, which is far away from the MPB, we have also observed that there are a large amount of Pb displacements along the monoclinic directions and they are able to rotate under external stimuli. The difference between this work and the previously mentioned reports is that the monoclinic distortions in Zr-rich and MPB compositions of PZT have different length scales. The monoclinic local polarizations are mainly observed at the unit cell level in our case. This suggests that there is certain structural flexibility in PZT in a wide composition range. With the Ti concentration increasing, this flexibility becomes more correlated, and therefore may contribute significantly to the overall high piezoelectric property of PZT.

See supplementary material for the fitted patterns using PDFFIT small-box modeling and RMC large-box modeling, full stereographic projection plots for Pb obtained from the RMC calculation and the distribution of the Pb-Pb displacement correlation coefficients from the RMC calculation.

This work was supported by the National Natural Science Foundation of China (Grant No. 61604123), Fundamental Research Funds for the Central Universities of China, a Grant-in-Aid for Young Scientists (B) from the

Ministry of Education, Culture, Sports, Science and Technology in Japan (Grant No. 15K1764) and the Shared Use Program of JAEA Facilities (Proposal No. 2014B-E14) with the approval of the Nanotechnology Platform Project supported by the Ministry of Education, Culture, Sports, Science and Technology, Japan. We thank the Research and Education Collaboration program in the Center for Frontier Science at Chiba University, Japan, to support the international collaboration between N.Z. and H.Y. Z.G.Y. acknowledges the support from the U.S. Office of Naval Research (ONR Grant Nos. N00014-12-1-1045 and N00014-16-3106) and the Natural Sciences and Engineering Research Council of Canada (NSERC Grant No. 203773). The synchrotron radiation experiments were performed at JAEA beamline BL14B1 in SPring-8 (Proposal No. 2014B-E14).

[1]MarketsandMarkets, *Piezoelectric Devices Market by Material (Piezoceramics, Piezopolymers, Piezocomposites, Piezocrystals), Product (Actuators, Transducers, Motors, Sensors, Generators), Application* (Industrial, Automotive, Healthcare, Consumer, 2017).
[2]B. Jaffe, R. S. Roth, and S. Marzullo, J. Appl. Phys. **25**, 809 (1954).
[3]B. Noheda, D. E. Cox, G. Shirane, J. A. Gonzalo, L. E. Cross, and S.-E. Park, Appl. Phys. Lett. **74**, 2059 (1999).
[4]D. Damjanovic, J. Am. Ceram. Soc. **88**, 2663 (2005).
[5]H. Fu and R. E. Cohen, Nature **403**, 281 (2000).
[6]B. Noheda, J. Gonzalo, L. Cross, and R. Guo, Phys. Rev. B **61**, 8687 (2000).
[7]H. Yokota, N. Zhang, A. E. Taylor, P. A. Thomas, and A. M. Glazer, Phys. Rev. B **80**, 104109 (2009).
[8]N. Zhang, H. Yokota, A. M. Glazer, and P. A. Thomas, Acta Crystallogr. B **67**, 386 (2011).
[9]N. Zhang, H. Yokota, A. M. Glazer, Z. Ren, D. A. Keen, D. S. Keeble, P. A. Thomas, and Z.-G. Ye, Nat. Commun. **5**, 5231 (2014).
[10]N. Zhang, H. Yokota, A. M. Glazer, D. A. Keen, S. Gorfman, P. A. Thomas, W. Ren, and Z.-G. Ye, IUCrJ **5**, 73 (2018).
[11]D. Vanderbilt and M. H. Cohen, Phys. Rev. B **63**, 94108 (2001).
[12]D. A. Keen and A. L. Goodwin, Nature **521**, 303 (2015).
[13]L. E. Cross, Ferroelectrics **76**, 241 (1987).
[14]M. S. Senn, D. A. Keen, T. C. A. Lucas, J. A. Hriljac, and A. L. Goodwin, Phys. Rev. Lett. **116**, 207602 (2016).
[15]J.-H. Ko, T. H. Kim, K. Roleder, D. Rytz, and S. Kojima, Phys. Rev. B **84**, 094123 (2011).
[16]G. Burns and F. H. Dacol, Solid State Commun. **42**, 9 (1982).
[17]R. Comès, M. Lambert, and A. Guinier, Acta Crystallogr. A **26**, 244 (1970).
[18]D. A. Keen, J. Appl. Crystallogr. **34**, 172 (2001).
[19]T. Egami and S. J. L. Billinge, *Underneath the Bragg Peaks: Structural Analysis of Complex Materials*, 2nd ed. (Elsevier, 2012).
[20]S. J. L. Billinge, J. Solid State Chem. **181**, 1695 (2008).
[21]C. L. Farrow and S. J. L. Billinge, Acta Crystallogr. **65**, 232 (2009).
[22]A. C. Dippel, N. Bindzus, D. Saha, J. T. Delitz, H. P. Liermann, N. Wahlberg, J. Becker, E. D. Bjesen, and B. B. Iversen, Z. Anorg. Allg. Chem. **640**, 3094 (2014).
[23]M. W. Terban, M. Johnson, M. Di Michiel, and S. J. L. Billinge, Nanoscale **7**, 5480 (2015).
[24]D. A. Keen, D. S. Keeble, and T. D. Bennett, Phys. Chem. Miner. **45**, 333 (2018).
[25]R. L. McGreevy, J. Phys.: Condens. Matter **13**, R877 (2001).
[26]Y. Yoneda, N. Matsumoto, Y. Furukawa, and T. Ishikawa, J. Synchrotron Radiat. **8**, 18 (2001).
[27]X. Qiu, J. W. Thompson, and S. J. L. Billinge, J. Appl. Crystallogr. **37**, 678 (2004).
[28]C. L. Farrow, P. Juhas, J. W. Liu, D. Bryndin, E. S. Božin, J. Bloch, T. Proffen, and S. J. L. Billinge, J. Phys.: Condens. Matter **19**, 335219 (2007).
[29]M. G. Tucker, D. A. Keen, M. T. Dove, A. L. Goodwin, and Q. Hui, J. Phys.: Condens. Matter **19**, 335218 (2007).
[30]H. Y. Playford, L. R. Owen, I. Levin, and M. G. Tucker, Annu. Rev. Mater. Res. **44**, 429 (2014).
[31]K. Németh, K. W. Chapman, M. Balasubramanian, B. Shyam, P. J. Chupas, S. M. Heald, M. Newville, R. J. Klingler, R. E. Winans, J. D. Almer, G. Sandi, and G. Srajer, J. Chem. Phys. **136**, 74105 (2012).
[32]R. E. Whitfield, T. R. Welberry, M. Paściak, and D. J. Goossens, Acta Crystallogr. A **70**, 626 (2014).
[33]R. E. Whitfield, D. J. Goossens, and T. R. Welberry, IUCrJ **3**, 20 (2016).
[34]B. Noheda, D. E. Cox, G. Shirane, R. Guo, B. Jones, and L. E. Cross, Phys. Rev. B **63**, 14103 (2000).
[35]J.-M. Kiat, Y. Uesu, B. Dkhil, M. Matsuda, C. Malibert, and G. Calvarin, Phys. Rev. B **65**, 64106 (2002).
[36]R. Guo, L. E. Cross, S.-E. Park, B. Noheda, D. E. Cox, and G. Shirane, Phys. Rev. Lett. **84**, 5423 (2000).
[37]B. Noheda, D. E. Cox, G. Shirane, S. E. Park, L. E. Cross, and Z. Zhong, Phys. Rev. Lett. **86**, 3891 (2001).